# Sentinel-1A: Analysis of FDBAQ Performance on Real Data

Pietro Guccione, Michele Belotti, Davide Giudici, Andrea Monti Guarnieri, *Member, IEEE*, and Ignacio Navas-Traver

## I. Introduction

SENTINEL-1 (S-1) is an imaging synthetic aperture radar (SAR) mission at C-band designed to supply all-weather day-and-night imagery to a number of operational Earth observation-based services. The mission is composed of a constellation of satellites for Earth observation, which was developed within the Copernicus program [previously known as Global Monitoring for Environment and Security (GMES)], i.e., the European program for the establishment of a European capacity for Earth observation [1].

The most relevant applications cover (but are not limited to) mapping in support of humanitarian aid in crisis situations, monitoring sea and ice zones (arctic, surveillance of marine environment, oil spill, marine traffic, etc.), and monitoring land surface for motion risks and for mapping [2], [3].

Four different measurement modes are available: the classical high-resolution Stripmap mode with a choice of six different swaths of 80-km width each, two medium-resolution wide-swath modes based on the progressive azimuth scanning principle [4], [5] [interferometric-wide-swath (IW) mode and extra-wide-swath (EW) mode] and a Wave mode designed for ocean applications.

Similar to many other modern SAR missions, S-1 produces a high output data rate and a large volume of data because of its large bandwidths, multiple polarizations, and the high duty cycle per orbit. S-1 is required to operationally acquire data for up to a quarter of an orbit (about 25 min), in dual polarization [6]; to this aim, it has two downlink channels of 260 Mb/s each, representing the upper limit for downloads done during the same acquisition.

The final mission archive is expected to exceed 10 PB.[1] Such demanding requirements led to the design of an onboard compression scheme that, exploiting the radar backscattering coefficient statistics, is able to exceed the image quality achieved in the previous fixed block adaptive quantizer (BAQ)-based C-band SAR missions [7], [8], while keeping the amount of acquired data to a manageable volume. FDBAQ has been designed with a flexible selection of bit rate allocation per sample [9]–[11] that largely achieves the average data rate within the specified channel limit. The FDBAQ implementation on S-1 produces an average bit rate comparable to that of BAQ-3 but with a significantly better image quality on bright targets, such as urban areas, and a slightly better image quality on more typical targets, such as global land surfaces [12]–[14].

As FDBAQ has been implemented for the first time on S-1, the capabilities of such a compression scheme have not been tested before on board during acquisition of real data. Simulation using real data [15] or preflight simulation and analysis were all based on a simplified processing scheme emulation as radar backscattering models and a global C-band radar echo mosaic taken from past missions. For this reason, the behavior of the compression scheme for every polarization, taking into account hardware constraints, such as the discretization of the values of receiver (RX) gain setting, effects of the 10-bit onboard quantizer and other minor instrument effects could not previously be included in the analysis. Their effect can be evaluated only using real S-1 data.

The purpose of this paper is to present the performance of FDBAQ on real products acquired during the first year of

Manuscript received March 25, 2015; revised May 23, 2015 and June 8, 2015; accepted June 12, 2015. The work has been carried out in the framework of the space segment activities of Sentinel-1.

P. Guccione is with the Dipartimento di Ingegneria Elettrica e Informazione, Politecnico di Bari, 70125 Bari, Italy (e-mail: pietro.guccione@poliba.it).

M. Belotti and D. Giudici are with Aresys Srl, 20132 Milan, Italy (e-mail: michele.belotti@aresys.it; davide.giudici@aresys.it).

A. Monti Guarnieri is with the Dipartimento di Elettronica, Informazione e Bioingegneria, Politecnico di Milano, 20132 Milan, Italy (e-mail: monti@elet.polimi.it).

I. Navas-Traver is with the ESA European Space Research Technology Centre (ESTEC), 2201 Noordwijk, The Netherlands (e-mail: ignacio.navas.traver@esa.int).

Color versions of one or more of the figures in this paper are available online.

[1] Source: http://www.dlr.de/eoc/en/desktopdefault.aspx/tabid-5258/15811_read-39583/

TABLE I
S-1 MAIN ACQUISITION PARAMETERS

| Mode | Off-nadir angle [deg] | Single Look Resolution (gr rg × az) | Swath Width | Polarization |
|---|---|---|---|---|
| Stripmap (S1,...,S6) | $[16.5 \div 41]$ | 5×5 m | 80 km | HH-HV, VV-VH |
| Interferometric Wide Swath (IW1,...,IW3) | $[26 \div 40]$ | 5×20 m | 250 km | HH-HV, VV-VH |
| Extra Wide Swath (EW1,....,EW5) | $[16.4 \div 41.2]$ | 20×40 m | 400 km | HH-HV, VV-VH |
| Wave Mode (WV1,WV2) | $[19.4 \div 22.4]$, $[31 \div 33.6]$ | 5×5 m | imagettes of 20×20 km | HH or VV |

activity of the instrument prior and after the end of the commissioning phase (CP; mid-September 2014). The performance of FDBAQ is highlighted in terms of quantization noise, signal-to-noise ratio (SNR), and average bit rate generated during product acquisition. The relative use of the different quantizers on the different kinds of land cover and the behavior of FDBAQ on cross-polarized acquisitions are analyzed in the next sections. The analysis started a few weeks after the launch and continued throughout the CP period and beyond. The results of the analysis during the CP have been used as recommendations for modifications of the onboard compression scheme parameters to further improve the compression performance and the image quality.

This paper is organized as follows: In Section II, an overview of the mission and the FDBAQ principles are presented. In Section III, a short analysis of FDBAQ during the CP is presented, and suggestions are made for further improvements of the compression scheme; in Section IV, the use of the quantizers, the subsequent effects on the average data rate, the behavior of FDBAQ at different polarizations, and the analysis of the image SNR are investigated. In Section V, this paper finishes with discussion and conclusions.

## II. OVERVIEW OF S-1 AND FDBAQ

S-1 is a C-band SAR satellite able to acquire data in four different selectable modes according to the different mission requirements. The satellite operates normally in yaw, pitch, and roll steering mode to compensate for Doppler shifts due to Earth rotation, and the antenna is able to cover an elevation look angle range from 16° (for S-1 Stripmap mode) to 41° (for the S-1 EW acquisition mode), providing a swath as large as 400 km in the EW mode. The S-1 acquisition parameters are summarized in Table I.

FDBAQ is a data compression algorithm that automatically selects a BAQ quantizer out of a set of $M = 5$ quantizers based on an estimation of the local signal-to-thermal-noise ratio estimated blockwise on the acquired data [16], thus exploiting the dynamic range of the radar echo power. Each quantizer is characterized by a fixed number of levels and by restitution values optimized for input data normally distributed with zero mean and unitary variance. The average bit rate and the quantization noise power are both a function of the number of levels and of the quantization interval.

The input to the onboard quantizer is modeled as the sum of the radar echo signal and the thermal noise referred to the output terminals of the receiving antenna and multiplied by the RX chain. Both are assumed complex circular zero-mean normal processes with powers of $P_{s,\mathrm{raw}}$ and $N_{\mathrm{th}}$, respectively. The SNR at the end of the RX accounts for the thermal and quantization noise power as follows:

$$\mathrm{SNR} = \frac{P_{s,\mathrm{raw}}}{N_{\mathrm{th}} + N_q}. \tag{1}$$

In the analysis, the realistic assumption is made that the quantization noise originates mainly from the granular effect of the quantizer and that the effect of clipping is negligible. This has been verified using real data (see Section III-A). On the basis of this assumption, the quantization noise can be expressed as a function of the input power and of the quantizer performance, given in terms of signal-to-quantization-noise ratio (SQNR), as follows:

$$N_q = \frac{P_{s,\mathrm{raw}} + N_{\mathrm{th}}}{\mathrm{SQNR}}. \tag{2}$$

The SNR in (1) can be rewritten using (2) as follows:

$$\mathrm{SNR} = \frac{\sigma_0}{\frac{N_{\mathrm{th}}}{\eta(r)} + \frac{\sigma_0 + N_{\mathrm{th}}/\eta(r)}{\mathrm{SQNR}}} \tag{3}$$

where the power of the signal at the receiving antenna output is described as the product of the radar backscattering coefficient $\sigma_0$ and the range-dependent scaling function $\eta(r)$, which includes all the range-variant and S-1 mission-specific parameters [17].

The S-1 sensitivity requirement is defined in terms of noise equivalent sigma naught $\sigma_{0,\min} \leq -22$ dB. In other words, the SNR (in db) is required to be greater or equal to the sigma naught (in db) $+22$ dB, i.e., SNR $\geq 0$ (in db), as follows:

$$\mathrm{SNR} = \frac{\sigma_0}{\frac{N_{\mathrm{th}}}{\eta(r)} + \frac{\sigma_0 + N_{\mathrm{th}}/\eta(r)}{\mathrm{SQNR}}} \geq \frac{\sigma_0}{\sigma_{0,\min}}. \tag{4}$$

The previous expression is depicted in Fig. 1. The selection of a specific quantizer defines the bit rate and the SQNR. The relation between $\sigma_0$ and SNR can be represented using (3). In Fig. 1, each continuous part of the blue curve represents the normalized backscattering coefficient interval, in which the chosen BAQ quantizer guarantees the condition in (4) with the minimum average bit rate. The FDBAQ switches the BAQ quantizers, where the image quality specification (red line) intersects the quantizer performance (blue curve). The switching positions are the *thresholds* between the quantizers [17]. The thresholds for the radar backscattering coefficient are transformed into input power thresholds using the radar equation $\eta(r)$, which is range and acquisition-mode dependent. The result is a table of rate selection thresholds varying with range and defined for each subswath. To avoid too much hardware complexity, the total range is divided into suitable range zones.

The set of quantizers loaded on board has been selected according to an optimization procedure aiming at minimizing

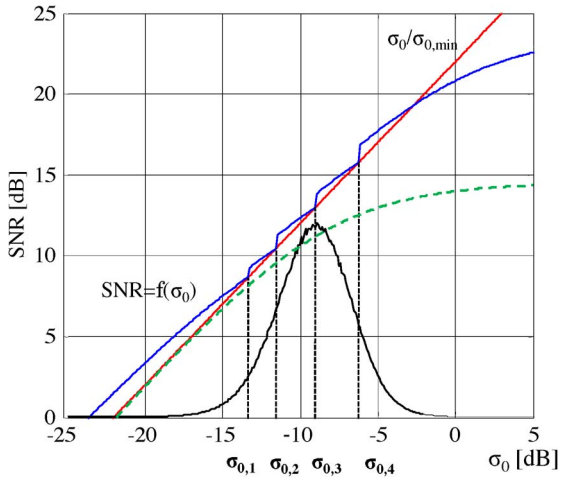


Fig. 1. SNR as a function of the radar backscattering coefficient. Red curve: the lower bound for the image quality; blue curve: SNR bound achieved by assuming FDBAQ quantization with five selectable quantizers as in S-1. The intersection of the red and blue curves gives the position of the radar backscattering coefficient thresholds. As a reference, the SNR as a function of radar backscattering coefficient for BAQ-3 is presented in green. The bell curve (in black, with no vertical scale) represents a typical $\sigma_0$ pdf.

the average data rate for the main operational Terrain Observation with Progressive Scan (TOPS)-IW mode, while keeping the noise equivalent sigma naught below $-22$ dB [12]. These quantizers produce an average bit rate that is a function of the statistics of the radar backscattering coefficient and of the position of the thresholds. The average bit rate may be estimated as the weighted sum of the five selected rates, the weights being defined by the probabilities that the radar backscattering coefficient is within each threshold interval. The probability is given by the area under the $\sigma_0$ probability density function (pdf) and within each threshold interval (see the black curve in Fig. 1).

### A. FDBAQ Concept Implementation in the S-1 Receiving Chain

The RX processing chain includes the 10-bit analog-to-digital converter (ADC), the digital down converter (DDC) that converts to zero frequency, the decimation filter, and the compression subsystem.

S-1 selects between five compression schemes (BAQ-3, BAQ-4, BAQ-5, FDBAQ, and no compression) as follows:

- *Echo data*, coming from land or sea, are compressed using FDBAQ. The five quantizers implemented in the FDBAQ compression scheme are uniform quantizers followed by an entropy encoder [18]. The bit rate is a variable and generally noninteger number of bits per sample (see Table III, where the bit rates have been computed for the hypothesis of a Gaussian data distribution with zero mean and unitary standard deviation).
- *Noise data*, used to provide a reference for the data mean and located at the beginning and end of each science product. The compression scheme is the Max–Lloyd BAQ (minimum quantization noise) with no entropy encoding. This scheme produces 3, 4, or 5 output bits for each input sample generated by the 10-bit ADC, corresponding to the BAQ-3, BAQ-4, and BAQ-5 compression modes, respectively. Since noise data in the current configuration are compressed following the BAQ-5 scheme, the bit rate is constant.
- *Calibration pulse samples* are not compressed. In this case, the bit rate is also constant, i.e., 10 bits/sample, at the output of the ADC.

Echo, noise, and calibration data are processed by the RX chain and packetized before downloading.

## III. CP Analysis of S-1A Data

### A. Quantizer Statistics

The analysis carried out on FDBAQ during the CP focused on three issues: 1) verify that the data statistics are as expected, i.e., Gaussian distributed with zero mean and spatially homogeneous within the estimation window; 2) evaluate the relative use of the five quantizers in the FDBAQ compression scheme; and 3) compare the average data rate with the expected ones. In spite of the preliminary nonoptimal setting of the instrument parameters during the CP, the assumption of a zero-mean Gaussian data distribution was confirmed.

The second and third issues are important to establish how FDBAQ image quality compares with BAQ-3 when the same bit rate is used. Results of the output bit and data rates achieved on some real acquisitions taken during the CP are in Table II (last two columns). The same table shows also the relative use of the quantizers, which is characterized by bit rate code (BRC). The low level of received signal forced FBAQ to use the first quantizer BRC0, for most of the time, leading to an almost constant bit rate of 2.54 bits/sample and the SQNR of 13.4 dB, as listed in Table III.

At the end of the CP, a decision was taken to increase the RX gain for all the modes, to achieve a more balanced use of the quantizers and a reduction in the quantization noise, at the cost of a slight increase in the bit rate, as detailed in Section III-B.

Finally, to verify the absence of clipping effects, several data sets with bright targets have been analyzed. The example reported here is an EW acquisition over a reference urban area (Tokyo, Japan). Considering the blocks with the highest standard deviation (i.e., the brightest blocks), the data distribution at the output of the ADC was analyzed to look for the possible presence of clipping effects. Fig. 2 shows the distribution of the I channel (normalized to 10 bits) of the brightest block, which is located in swath EW2. The distribution of levels in the range $[-512, 511]$ suggests the absence of clipping.

The optimization of FBAQ performance needs a careful evaluation of the bit rate. To this aim, simulations were carried out on a simplified S-1 processing chain. Simulation was based on real S-1 geometry and a number of patches of radar backscattering coefficient extracted from an HH-polarization C-band mosaic derived from Environmental Satellite (ENVISAT) ASAR Global Monitoring Mode (GMM) acquisitions [19]. Simulated products have been prepared for all the S-1 acquisition modes, except for Wave mode, for which the data rate is too low to be critical. A number of 19 patches have been used on three different scenarios representative of the world surface cover types: desert, forest, crops, cities, and ice. The average bit rate [in bits per sample] has been estimated, by accounting for the input power taken from the acquired scenes (function of

TABLE II
RELATIVE USE OF QUANTIZERS AND AVERAGE BIT–DATA RATES FOR A SELECTED SET OF CP ACQUISITIONS

| id # | Area/description | Mode | Acq. Date and time | Pol | BRC0 | BRC1 | BRC2 | BRC3 | BRC4 | Av bit rate | Av data rate |
|---|---|---|---|---|---|---|---|---|---|---|---|
| | | | | | $w_{BRC}$ [%] | | | | | [bit/sample] | [Mbit/sec] |
| 1 | North-West of Iceland, sea | EW | 20140417 18:56:59 | HH | 97.51 | 2.05 | 0.43 | 0.00 | 0.00 | 2.5438 | 61.40 |
| 2 | The Netherlands, sea | IW | 20140512 05:48:13 | HV | 99.95 | 0.03 | 0.02 | 0.00 | 0.00 | 2.5358 | 188.69 |
| 3 | Eritrea, Djibouti, Red sea | IW | 20140417 02:59:05 | VV | 98.67 | 1.31 | 0.02 | 0.00 | 0.00 | 2.5390 | 191.96 |
| 4 | Eritrea, Djibouti, Red sea | IW | 20140417 02:59:05 | VH | 100.0 | 0.00 | 0.00 | 0.00 | 0.00 | 2.5356 | 202.66 |
| 5 | South Germany, Black Forest | S4 | 20140411 05:31:20 | HH | 99.49 | 0.39 | 0.11 | 0.01 | 0.00 | 2.5374 | 182.80 |
| 6 | Inner lands of Netherlands | S6 | 20140419 05:44:05 | HV | 99.99 | 0.01 | 0.00 | 0.00 | 0.00 | 2.5356 | 182.52 |
| 7 | Greenland, Arctic sea | EW | 20140421 10:12:45 | HH | 70.50 | 12.38 | 11.44 | 5.17 | 0.50 | 2.7112 | 64.04 |
| 8 | Greenland, Arctic sea | EW | 20140421 10:12:45 | HV | 98.04 | 1.68 | 0.28 | 0.00 | 0.00 | 2.5418 | 61.97 |

TABLE III
PROPERTIES OF THE QUANTIZERS USED IN FDBAQ/BAQ IN IDEAL CONDITIONS [12], [18]

| Quantizer | # levels | $q_{BRC}$ [bit/sample] | SQNR [dB] |
|---|---|---|---|
| FDBAQ BRC0 | 8 | 2.5356 | 13.3718 |
| FDBAQ BRC1 | 10 | 2.7910 | 14.9823 |
| FDBAQ BRC2 | 14 | 3.2234 | 17.4552 |
| FDBAQ BRC3 | 20 | 3.6310 | 20.1206 |
| FDBAQ BRC4 | 32 | 4.2376 | 23.6851 |
| Max-Lloyd BAQ-3 | 8 | 3 | 14.6168 |
| Max-Lloyd BAQ-4 | 16 | 4 | 20.2241 |
| Max-Lloyd BAQ-5 | 32 | 5 | 26.0223 |

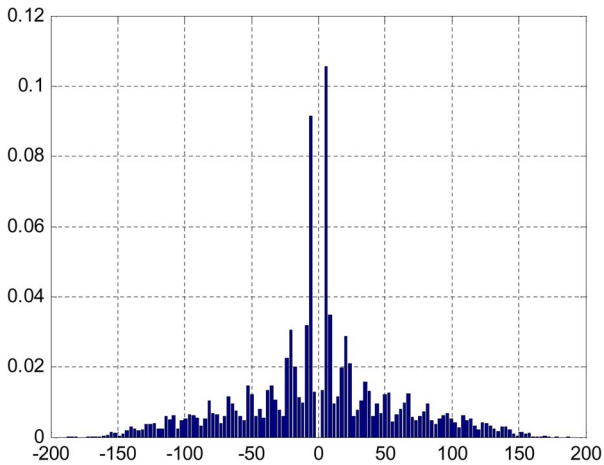


Fig. 2. Distribution of real data (I channel) at the output of ADC for the brightest block of data set ID 000F87, taken on Tokyo urban area and using the EW-HH mode.

the real radar backscattering coefficient of the scenarios) and the theoretical number of bits per sample provided by each quantizer (see Table III), assuming Gaussian zero-mean data distribution. The average bit rate results are as follows:

### B. CP/Post-CP Bit Rate Analysis

Making better use of the available dynamic range can be achieved by optimal tuning of the RX gain. This leads to a reduction in the quantization noise originating from both the 10-bit ADC and the FDBAQ compression and to a sensible reduction in the impact of some nonlinearities and spurious effects within the RX.

TABLE IV
REAL AVERAGE DATA RATE (CP/POST-CP) AND ESTIMATES (POST-CP)

| Swath | CP Rx Gain [dB] | Av. Data Rate [Mbit/sec] (CP) | post-CP Rx Gain [dB] | Estim. Av. Data Rate [Mbit/sec] (post-CP) | Effect. Av. Data Rate [Mbit/sec] (post-CP) |
|---|---|---|---|---|---|
| S1 | -9.0 | 251.73 | -6.0 | 279.25 | 271.5 |
| S2 | -8.5 | 203.13 | -6.0 | 220.36 | 213.36 |
| S3 | -8.0 | 223.93 | -6.0 | 230.78 | 222.56 |
| S4 | -7.0 | 185.8 | -6.0 | 187.59 | 188.58 |
| S5 | -6.5 | 205.38 | -6.0 | 204.73 | 208.04 |
| S6 | -6.5 | 177.58 | -6.0 | 177.08 | 178.39 |
| IW1 | -7.5 | | -4.0 | | |
| IW2 | -7.0 | 192.21 | -4.0 | 216.90 | 194.89 |
| IW3 | -6.5 | | -4.0 | | |
| EW1 | -4.0 | | 0.0 | | |
| EW2 | -3.0 | | 0.0 | | |
| EW3 | -3.0 | 60.36 | 0.0 | 65.72 | 62.32 |
| EW4 | -3.0 | | 0.0 | | |
| EW5 | -3.0 | | 0.0 | | |
| WV1 | -9.5 | 9.88 | -6.5 | n/a | 11.8 |
| WV2 | -7.0 | 6.76 | -6.5 | n/a | 6.7 |

$$\bar{n} = \frac{\sum_{m=0}^{4} w_{\mathrm{BRC}} q_{\mathrm{BRC}}}{\sum_{m=0}^{4} w_{\mathrm{BRC}}} \quad \text{[bits/sample]} \tag{5}$$

where $w_{\mathrm{BRC}}$ are the relative usage of the quantizers, i.e., $\sum_{\mathrm{BRC}} w_{\mathrm{BRC}} = 1$ (the index BRC goes from 0 to 4), and $q_{\mathrm{BRC}}$ [in bits per sample] are in Table III. The average data rate [in megabits per second] is finally determined considering the number of bits per sample and the number of samples acquired in a second. The average data rate is mode dependent because it is a function of the swath width (in samples per line) and of the pulse repetition frequency (in lines per second). The estimation of the average data rate for all the modes was achieved at different values of RX gain. The purpose was to evaluate the impact on the data rate of the modification of the RX gain prior to its use. We found that the data rate has a linear relation with the RX gain measured in natural units and that the slope of such a relation is higher for swaths with lower off-nadir acquisition angles.

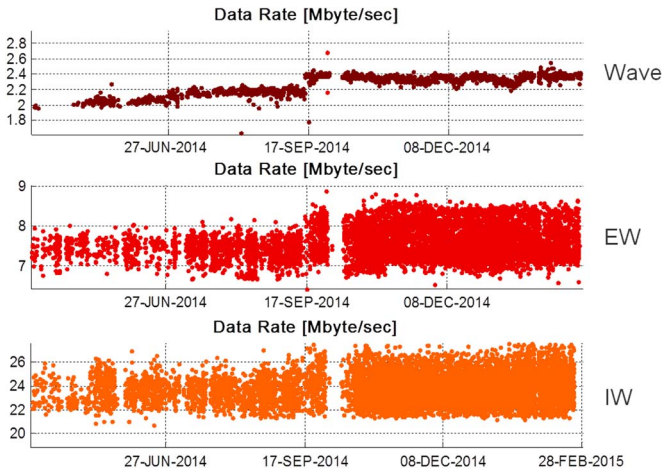


Fig. 3. Data rate [in megabytes per second] time series from satellite launch up to the end of February 2015 for Wave, TOPS-IW, and TOPS-EW acquisition modes.

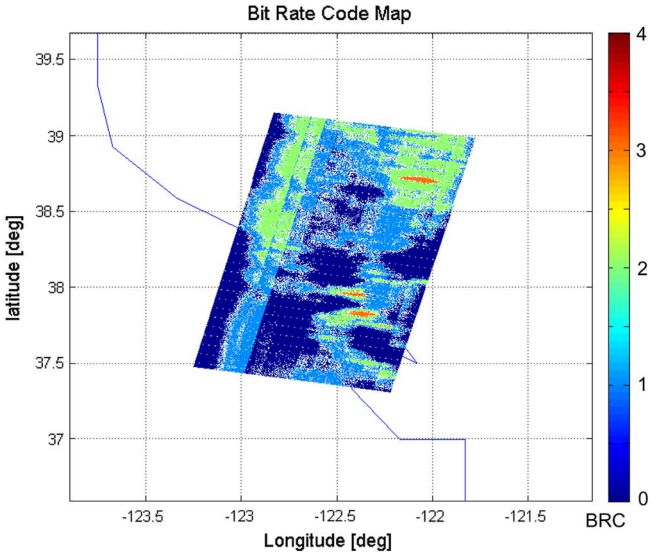


(a)

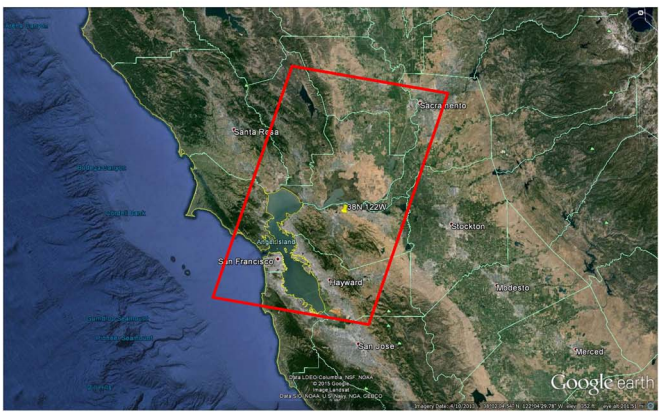


(b)

Fig. 4. San Francisco area acquired using Stripmap S1. (a) BRC geolocated map; (b) corresponding Google Earth map. The geolocation is not accurate since the Doppler centroid has not been compensated. The values of BRC go from 0 to 4 (4 is the highest quantizer).

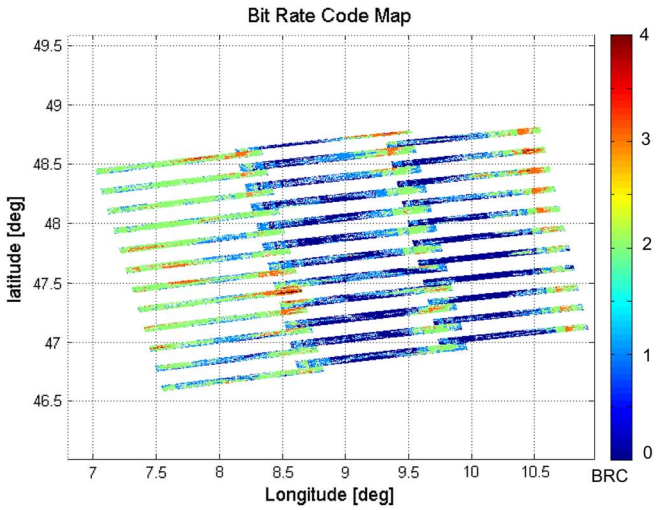


(a)

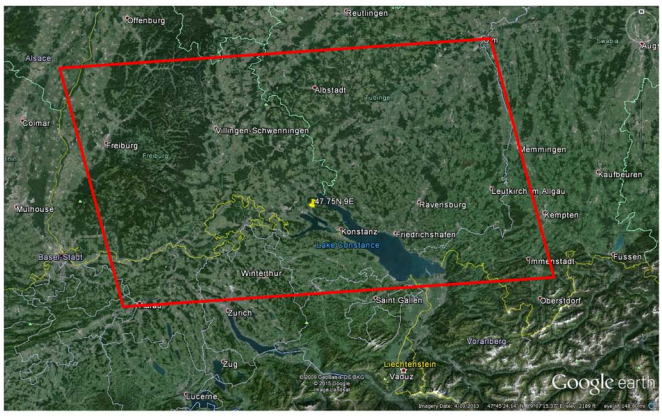


(b)

Fig. 5. Black Forest area acquired using IW mode. (a) BRC geolocated map; (b) corresponding Google Earth map. The geolocation is not accurate since the Doppler centroid has not been compensated. The values of BRC go from 0 to 4 (4 is the highest quantizer).

Table IV presents, for each swath, the following: 1) the values of the RX gain before the increase (numbers are given with respect to a reference value); 2) the average data rate obtained during a large number of real acquisitions (more than 18 800 acquired from April 12 to August 20,2014) taken during the CP period; 3) the RX gain set at the end of the CP (the difference between column 4 and column 2 gives the gain increase); 4) the estimated data rate evaluated by simulation; 5) the average data rate obtained during a large number of real acquisitions (about 10 000) taken from September 20, 2014, to February 2, 2015 (i.e., after mid-September 2014). Estimation in the fifth column was done by interpolation, using the results of simulations and the linear relation previously mentioned.

The actual value of RX gain loaded on board has been identified during the CP. After the onboard gain change, only the Stripmap S1 mode exceeds the upper limit for downloads done during the same acquisition (260 Mb/s).

From a comparison between estimated and actual average data rates in the post-CP phase, in some cases, the latter was found lower than the predicted one and, in one case in the S3 mode, lower than during the CP phase. This can be explained by the significant nadir return that affected CP data takes.

The time series of the data rate (in megabytes per second) is sketched in Fig. 3 for three different modes. The horizontal axis

TABLE V
RELATIVE USE OF QUANTIZERS AND AVERAGE BIT–DATA RATES FOR A SELECTED SET OF POST-CP ACQUISITIONS

| id # | Area/description | Mode | Acq. Date and time | Pol | BRC0 | BRC1 | BRC2 | BRC3 | BRC4 | Av bit rate | Av data rate |
|---|---|---|---|---|---|---|---|---|---|---|---|
| | | | | | $w_{BRC}$ [%] | | | | | [bit/sample] | [Mbit/sec] |
| 1 | South Germany, Black Forest | IW | 20141010 05:34:15 | VV | 6.93 | 30.07 | 45.20 | 15.81 | 2.00 | 3.1880 | 230.60 |
| 2 | South Germany, Black Forest | IW | 20141010 05:34:15 | VH | 99.59 | 0.366 | 0.035 | 0.0047 | 3.2e-4 | 2.6258 | 190.09 |
| 3 | South Germany, Black Forest | IW | 20141205 17:15:03 | VV | 30.04 | 26.18 | 36.07 | 7.31 | 0.39 | 3.0261 | 214.46 |
| 4 | South Germany, Black Forest | IW | 20141205 17:15:03 | VH | 99.91 | 0.0877 | 0.00168 | 1.11e-4 | 0 | 2.6371 | 187.01 |
| 5 | San Francisco area | S1 | 20141205 14:23:33 | VV | 40.77 | 40.11 | 18.40 | 0.72 | 0.0018 | 2.8165 | 272.05 |
| 6 | Greenland | EW | 20141205 20:36:27 | HH | 51.31 | 12.92 | 21.40 | 14.19 | 0.19 | 3.0051 | 68.20 |
| 7 | Greenland | EW | 20141205 20:36:27 | HV | 90.59 | 6.04 | 3.36 | 2.37e-4 | 0 | 2.8369 | 64.43 |
| 8 | North Korea, China | IW | 20141207 22:20:18 | VV | 67.01 | 19.20 | 8.94 | 3.28 | 1.58 | 2.8205 | 199.63 |

reports the acquisition date since satellite launch and up to the end of February 2015. In the case of the Wave mode, the dispersion of the data rate is much smaller since the acquisitions are done over oceans, where the variability of the radar backscattering coefficient is more limited. Particularly for Wave mode, clear variations of data rate in the CP period can be appreciated: they are due to initial adjustments of the satellite orbit. Finally, the change in trend is visible after September 16, for all the modes, when the new gain values were uploaded on board. For acquisition modes different from Wave mode, the high variability in the bit rate shows that a dynamic compression scheme as FDBAQ is a good choice to match the large variability of the radar backscattering coefficient, due to different land cover types and different acquisition conditions, i.e., incidence angle, polarization, season, and soil moisture content.

## IV. POST-CP ANALYSIS OF S-1A DATA

### A. Relative Use of BAQ Quantizers

*1) Geographical Distribution of Quantizer Use:* Both FDBAQ and BAQ are based on the hypothesis that input data have a Gaussian distribution with zero mean and space-variant standard deviation. It is for this reason that both the compression schemes estimate the input power on a range block basis, assuming a locally stationary distribution. This way, the quantizer selection reflects the relative difference in input power at the receiving antenna output.

Figs. 4 and 5 illustrate two cases in the post-CP period. In Fig. 4(a), the BRC for an acquisition taken using Stripmap S1 mode on the area around San Francisco is mapped in geographic coordinates. In Fig. 5(a), the BRC map is shown on the Black Forest in Germany acquired using IW mode.[2] The BRC of each quantization block is imaged as integer numbers going from 0 to 4 (0 for the quantizer with 8 levels and 4 for the quantizers with 32 levels, according to Table III) and approximately mapped on geographic coordinates. The acquisitions sketched in Figs. 4 and 5 are the #5 (for Stripmap S1) and #3 (for TOPS-IW) in Table V, respectively.

As can be seen, the fourth and fifth quantizers (BRC3 and BRC4) are used particularly on urban areas (corresponding to the orange-red spots in the two figures). This gives, on those areas, an SNQR improvement of at least 5.6 dB compared to a BAQ-3, while the average bit rate is kept below or about 3 bits/sample for the total image.

*2) Improvement After the End of CP:* At the end of the CP (mid-September 2014), the RX gain for all the modes was increased. Such increase produced a reduction in the quantization noise and an increase in the average bit and data rates.

The effect of such an increase can be appreciated by inspection of Tables II (CP period) and V (post-CP period). In Table V, we have an improvement in the use of quantizers, with the highest number of bits on the same area. The modification of the use of BRC can be appreciated also by visual inspection of Fig. 6, where the geographical distribution of the BRC is presented for two acquisitions covering approximately the same area (Black Forest in Germany). On the left is the BRC distribution before the RX gain increase; on the right is the BRC distribution after the gain increase.

A comparison of Tables II and V shows that the copolarization acquisitions now make a more balanced use of the quantizers because of the increase in the onboard RX gain. However, the cross-polarization acquisitions still suffer from such an impairment. This issue is discussed in Section IV-B.

### B. FDBAQ Behavior on Cross-Polarized Acquisitions

S-1 can operate in dual polarization. In this mode, the instrument transmits a single vertical or horizontal linearly polarized electromagnetic wave and receives both vertical and horizontal polarized waves on two separate channels carrying different information about the area under observation [20], [21]. In this operational mode, the best performance would be achieved if optimization of the FDBAQ rate selection thresholds would be done separately for co- and cross-polarization. Currently, on board the S-1A, the compression is performed separately on the two receiving channels, while a common set of compression parameter tables is used. Since compression parameters are selected for the copolarization only, some performance reduction is expected for cross-polarized products.

This is confirmed by direct observation of the quantizer use of the products. In Table V, the quantizer distribution can be observed in the dual-polarization products (products 1 and 2 and products 3 and 4 in V transmission and IW mode; products 6 and 7 in H transmission and EW mode). It is noted, for

[2]Please note that, for TOPS modes in Figs. 5(a) and 6, the BRC map is imaged in the original burstwise acquisition since the intention is just to sketch the quantizer use in the approximate location during acquisition.

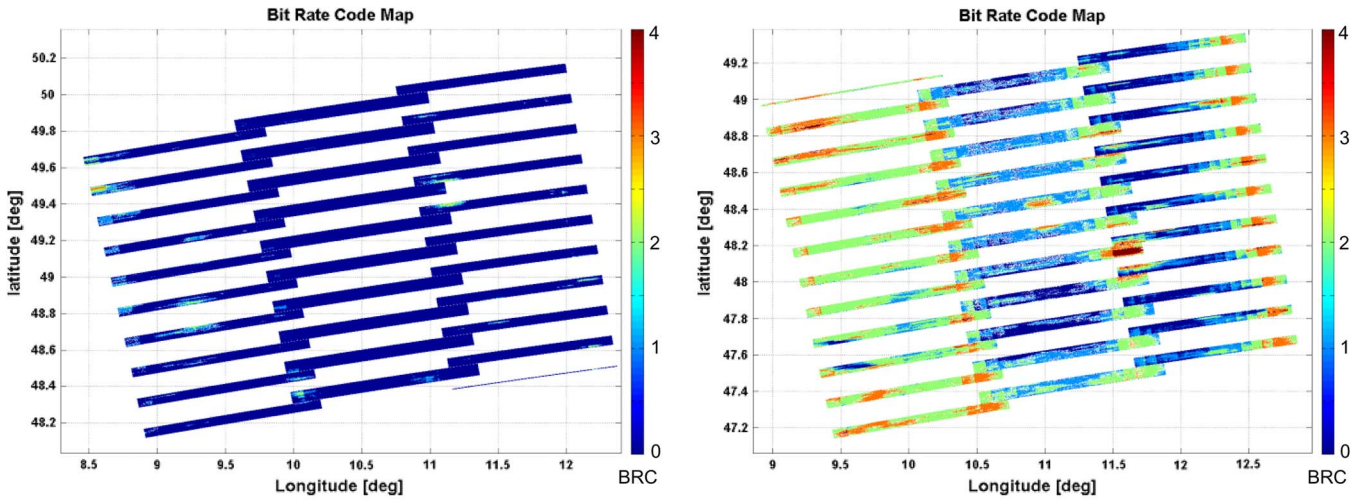


Fig. 6. BRC usage on the Black Forest in Germany for IW-HH acquisition before (April 19, 2014; left) and after (October 13, 2014; right) the increase in RX gain.

example, that in the case of product 2 (IW, VH), the first quantizer is mostly used, since the rate selection thresholds are higher than the input power level. The cross-polarized radar backscattering coefficient is, on average, 7–10 dB lower than the corresponding copolarized radar backscattering coefficient. This makes the image acquired in cross-polarized mode very similar to a BAQ-3 acquisition, the main difference being that the uniform quantizer followed by an entropic encoder, which is implemented in the FDBAQ, produces higher quantization noise [18] and lower average bit rate (≈2.63 bits/sample; see the column of the Average Bit Rate for rows 2 and 4).

Increase in the quantization noise is particularly visible in products with abrupt changes of radar backscattering coefficient (for example, when a city is imaged in a coastal area) or when a few bright targets are surrounded by a dark background. Due to the blockwise selection of the quantizer, it may happen that a low quantizer is assigned to such targets, even if very bright. This means less bits, smaller dynamic range, and more quantization noise.

This can be appreciated by visual inspection when focused dual-polarized products are compared to each other. The cross-polarized images in Fig. 7, at the right, have been produced starting from raw data compressed using FDBAQ (as the copolarized, at the left) whereby the first quantizer is used for more than 99% of the time. The quantization noise is represented by a halo in the sea [for both Fig. 7(b) and (d)] or on the dark background in Fig. 7(f). A reduction in dynamic range is also apparently causing loss of details in the urban area [compare Fig. 7(a) with (b) and Fig. 7(e) with (f)]. A simple explanation of the halo can be given in terms of processing of quantization noise, which is higher in the images on the right, in Fig. 7. In fact, since quantization noise does not focus, it remains extended over the unfocused resolution cell. Its effects are more evident particularly in the images where the first quantizer has been mainly used.

We stress again that the artifacts in Fig. 7(b), (d), and (f) are basically due to the limits of BAQ and not due to FDBAQ, since in cross-polarization mode, FDBAQ is basically a fixed BAQ (see the analysis on the use of quantizers). Such an effect is expected, subject to further theoretical and experimental analysis, to represent the effects of quantization noise.

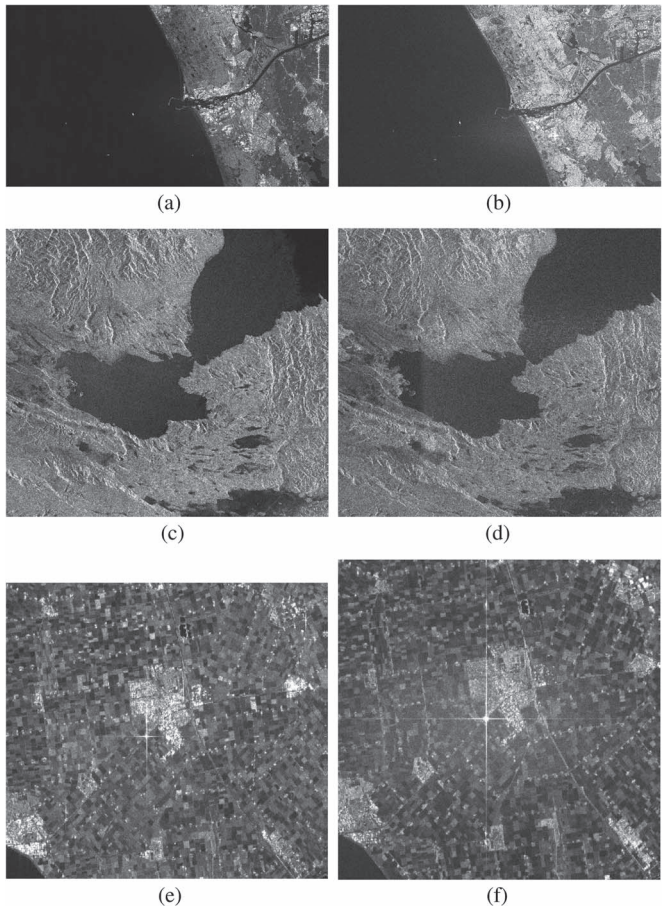


Fig. 7. Comparison of dual-polarization focused products. Details on The Netherlands area (The Hague city) acquired with S6 mode in (a) HH and (b) HV. Details on the Djibouti area, Eritrea (Lake Goubet) acquired with the IW mode in (c) VV and (d) VH. Detail on the Netherlands area acquired with S6 mode, over an active transponder, in (e) HH and (f) HV.

### C. SNR Analysis

Using (3), it is possible to derive the SNR for the acquisitions. SNR better expresses the quality of an image since it is a function not only of the quantizer choice but also of the level of radar backscattering coefficient. To simplify the analysis, the

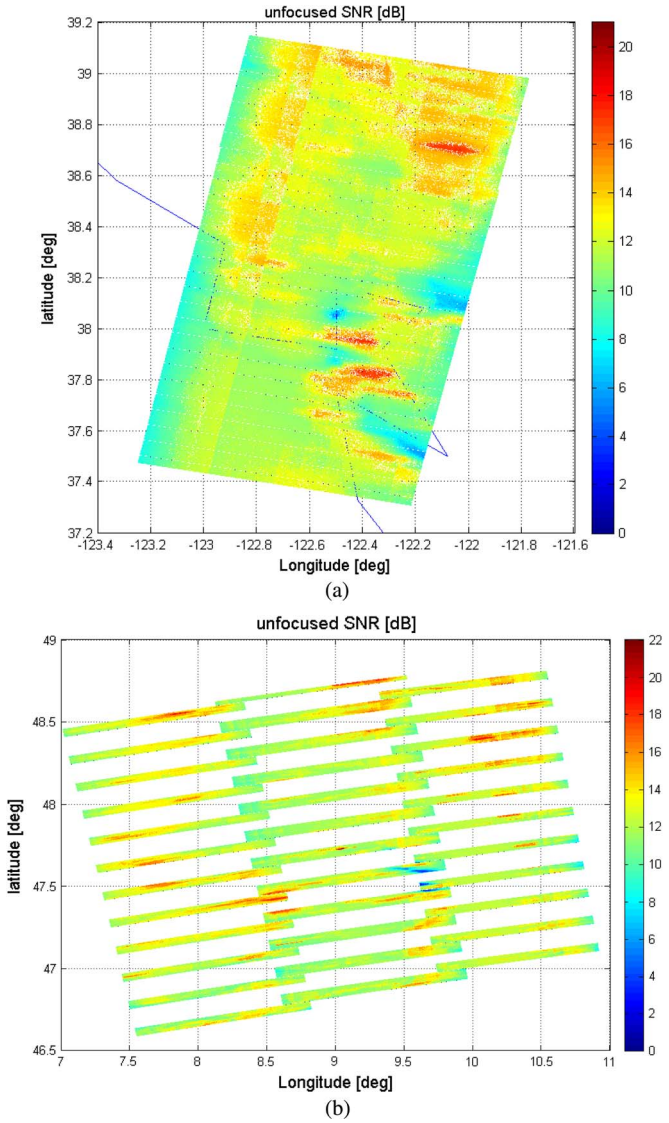


Fig. 8. (a) San Francisco and (b) Black Forest acquisition raw SNR maps. The acquisitions are the same as already sketched in Figs. 4 and 5, respectively.

nominal SQNR that can be assigned to each quantizer is used, according to Table III. For each range block, the input power at the receiving antenna output $P_{s,\mathrm{raw}} + N_{\mathrm{th}}$ is used to estimate the quantization noise, taking the information of the selected quantizer to get an estimate of SQNR (from Table III). Finally, to estimate $N_{\mathrm{th}}$, the noise data lines included in hundreds of products for all the modes and polarizations are used. With this, the unfocused SNR can be determined as follows:

$$\mathrm{SNR} = \frac{P_{s,\mathrm{raw}}}{N_{\mathrm{th}} + \frac{P_{s,\mathrm{raw}}+N_{\mathrm{th}}}{\mathrm{SQNR}}}. \tag{6}$$

The SNR maps for San Francisco and the Black Forest are sketched in Fig. 8. As expected, the urban areas show the highest SNR.

Furthermore, it is possible with some approximation, to emulate the effect of other compression schemes on the same acquisition. To do this, (6) is used with the substitution of the SQNR of a different quantization. FDBAQ is compared with the following: 1) BAQ-3 (whose SQNR is 14.62 dB) and 2) entropy-constrained BAQ (ECBAQ) [22], whose SQNR for

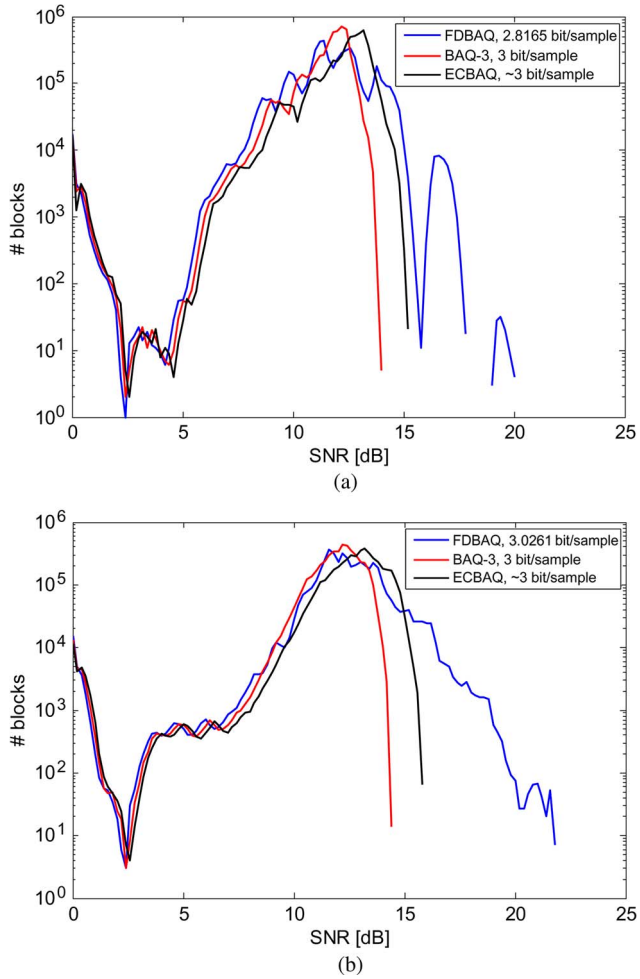


Fig. 9. Semilog plot of the raw SNR histograms for (a) San Francisco and (b) Black Forest acquisitions. FDBAQ, BAQ-3, and ECBAQ are compared.

a bit rate of about 3 bits/sample is 16.17 dB. Histograms of the two acquisitions for FDBAQ and emulated BAQ-3 and ECBAQ are in Fig. 9. As expected, FDBAQ is very similar to BAQ-3 or ECBAQ for most of the targets (the central part of the histogram) or for the dark targets (the ones with low SNR) but shows higher performance, i.e., up to 6 dB, for the few targets with high SNR (in both the cases supposedly the urban areas). The histogram for BAQ-5 is not reported since it clearly outperforms FDBAQ but at the cost of a very high bit rate.

## V. Discussion and Conclusion

In this paper, the performance and capabilities of the FDBAQ compression scheme have been shown using S-1 real data acquired in a period of ten months. The onboard FDBAQ quantizer, a dynamic evolution of the traditional BAQ, greatly improves the SNR in limited high-reflectivity areas, such as cities, and does not worsen the quality of dark targets when it is compared to the BAQ-3. In fact, FDBAQ exploits the capability to adapt the compression performance to the instantaneous backscatter level. FDBAQ performance is then similar to BAQ-3, in terms of the average bit rate, but much better over bright areas, where the level of quantization noise is similar to that of BAQ-5. Further improvement of data quality could be obtained by considering dedicated rate selection threshold tables for co- and cross-polarization channels.

## ACKNOWLEDGMENT

The authors would like to thank the ESA Sentinel-1 Commissioning Phase Team, AirBus Defence and Space (D&S), Systems is a British multinational defence, security and aerospace company (BAE) Systems Advanced Technology Centre, and Thales Alenia.

## REFERENCES

[1] R. Torres *et al.*, "GMES Sentinel-1 mission," *Remote Sens. Environ.*, vol. 120, pp. 9–24, May 2012.
[2] P. Snoeij *et al.*, "Sentinel-1, the GMES radar mission," in *Proc. IEEE RADAR*, May 2008, pp. 1–5.
[3] M. Davidson *et al.*, "Sentinel-1 mission overview," in *Proc. EUSAR*, Jun. 2010, pp. 1–4.
[4] P. Potin, B. Rosich, J. Roeder, and P. Bargellini, "Sentinel-1 mission operations concept," in *Proc. IEEE IGARSS*, Jul. 2014, pp. 1465–1468.
[5] A. Panetti *et al.*, "Copernicus Sentinel-1 satellite and C-SAR instrument," in *Proc. IEEE IGARSS*, Jul. 2014, pp. 1461–1464.
[6] E. Attema *et al.*, "Analysis of Sentinel-1 mission capabilities," in *Proc. EUSAR*, Jun. 2010, pp. 1–4.
[7] R. Kwok and W. T. K. Johnson, "Block adaptive quantization of Magellan SAR data," *IEEE Trans. Geosci. Remote Sens.*, vol. 27, no. 4, pp. 375–383, Jul. 1989.
[8] I. H. McLeod, I. G. Cumming, and M. S. Seymour, "ENVISAT ASAR data reduction: Impact on SAR interferometry," *IEEE Trans. Geosci. Remote Sens.*, vol. 36, no. 2, pp. 589–602, Mar. 1998.
[9] M. Martone, B. Brautigam, and G. Krieger, "Azimuth-switched quantization for SAR systems and performance analysis on tanDEM-X data," *IEEE Geosci. Remote Sens. Lett.*, vol. 11, no. 1, pp. 181–185, Jan. 2014.
[10] U. Benz, K. Strodl, and A. Moreira, "A comparison of several algorithms for SAR raw data compression," *IEEE Trans. Geosci. Remote Sens.*, vol. 33, no. 5, pp. 1266–1276, Sep. 1995.
[11] H. Zhang, J. Chen, J. Li, H. Zeng, and W. Yang, "Segmented BAQ algorithm for SAR raw data of strong target in weak background," in *Proc. APSAR*, Sep. 2013, pp. 470–472.
[12] E. Attema *et al.*, "Flexible dynamic block adaptive quantization for Sentinel-1 SAR missions," *IEEE Geosci. Remote Sens. Lett.*, vol. 7, no. 4, pp. 766–770, Oct. 2010.
[13] P. Guccione, C. Cafforio, and A. Monti Guarnieri, "Optimal block quantization for SAR data," in *Proc. Radar Conf.*, May 2010, pp. 348–353.
[14] E. Attema *et al.*, "Sentinel-1 flexible dynamic block adaptive quantizer," in *Proc. EUSAR*, Jun. 2010, pp. 1–6.
[15] E. Malz, R. Scheiber, J. Mittermayer, P. Snoeij, and E. Attema, "Sentinel-1 FDBAQ performance validation using TerraSAR-X data," in *Proc. IGARSS*, Jul. 2012, pp. 1629–1632.
[16] J. Mittermayer *et al.*, "TerraSAR-X system performance characterization and verification," *IEEE Trans. Geosci. Remote Sens.*, vol. 48, no. 2, pp. 660–676, Feb. 2010.
[17] P. Guccione and A. Monti Guarnieri, "A space adaptive quantizer for spaceborne SAR," *IEEE Trans. Geosci. Remote Sens.*, vol. 49, no. 10, pp. 3564–3573, Oct. 2011.
[18] A. Gersho, "Principles of quantization," *IEEE Trans. Circuits Syst.*, vol. 25, no. 7, pp. 427–436, Jul. 1978.
[19] C. Caspar *et al.*, "Generation of ENVISAT ASAR Mosaics accessible on-line," in *Proc. IEEE IGARSS*, Jul. 2007, pp. 1405–1408.
[20] Y. Oh, K. Sarabandi, and F. T. Ulaby, "An empirical model and an inversion technique for radar scattering from bare soil surfaces," *IEEE Trans. Geosci. Remote Sens.*, vol. 30, no. 2, pp. 370–381, Mar. 1992.
[21] P. C. Dubois, J. Van Zyl, and T. Engman, "Measuring soil moisture with imaging radars," *IEEE Trans. Geosci. Remote Sens.*, vol. 33, no. 4, pp. 915–926, Jul. 1995.
[22] T. Algra, "Data compression for operational SAR missions using entropy-constrained block adaptive quantisation," in *Proc. IEEE IGARSS*, Jun. 2002, vol. 2, pp. 1135–1139.